Sub-structure-based 'three-tiered' finite element approach to soil-masonry-wall interaction for light seismic motion

Longo, Michele; Sousamli, Marianthi; Korswagen, Paul; van Staalduinen, Piet; Rots, Jan G.

DOI
10.1016/j.engstruct.2021.112847

Publication date
2021

Document Version
Final published version

Published in
Engineering Structures

Engineering Structures 245 (2021) 112847

Contents lists available at ScienceDirect

Engineering Structures

journal homepage: www.elsevier.com/locate/engstruct

Sub-structure-based 'three-tiered' finite element approach to soil-masonry-wall interaction for light seismic motion

Michele Longo, Marianthi Sousamli, Paul A. Korswagen *, Piet van Staalduinen, Jan G. Rots

Faculty of Civil Engineering and Geosciences, Delft University of Technology, Netherlands

ARTICLE INFO

Keywords:
FEM modelling
Soil modelling
Seismic motion propagation
Soil-structure interaction
Light damage
Masonry

ABSTRACT

Recent, light earthquakes induced by the extraction of gas in the north of the Netherlands have been linked to light, mostly aesthetic damage of the traditional masonry structures in the region; this is also connected to economic losses and societal unrest. To be able to accurately assess the light damage, detailed finite element models are necessary and need to include realistic soil movement, wave propagation, and soil-structure interaction boundaries. Moreover, the minute deformation of the soil, including the rocking and translational components of seismic ground motion, has shown to be influential to light damage. Consequently, this study has pursued the definition of efficient soil-structure interaction boundaries to implement in finite element models of buildings.

A methodology, following the sub-structure method for the seismic Soil-Structure-Interaction (SSI) is defined and presented. The soil-structure-system is divided into three sub-systems: the far-field soil, the near-field soil and the superstructure. First, a 3 km deep and 8 km wide, plane-strain model of the soil is employed to study the behaviour of the soil at the surface due to deep, simplified seismic events. The soil model is linear-elastic since only light seismic excitations are considered. Next, a smaller, 30 × 300 m (shallow) soil model with a building on top, is given boundary elements calibrated to replicate the behaviour observed at the surface in the larger model. Finally, 2D models of masonry façades set on the intermediate soil model are used to reduce the soil-structure interaction to representative interface elements. The models are matched in terms of dynamic behaviour, strains, cracking, and displacements, and the behaviour is compared to existing ground motion data for the Zeerijp and Westerwijtwerd earthquakes. It is demonstrated that the equivalent interface allows efficient modelling of seismic excitations considering a detailed soil-structure interaction for complex, smeared non-linear, time-history analyses of wall models to assess (light) damage in probabilistic studies. Models with this equivalent interface show greater damage than comparison models without it.

1. Introduction

The interaction of soil and structure can be paramount when assessing the impact of vibrations on a structure. The soil may dampen or amplify the effect of the vibrations [1], it may deform or provide a stiff reaction to the foundation of the structure [2], or participate in some of the failure mechanisms of the structure [3]. An understanding of the behaviour of the soil, alone but also together with the structure, is thus key for a successful and accurate analysis of a structure.

It is often assumed by structural engineers that the motion of the base of the structure is the same as the free-field motion, which is the motion of the ground in the absence of surrounding buildings. Even though this assumption stands true in the case of structures built directly on rigid ground (e.g.. rock), in the case of structures founded on deformable soil (e.g. sand or clay) the foundation motion and the free-field motion are different. This difference in the input motion at the foundation also leads to a difference in the response of the structure [4]. The approaches that are usually adopted for the simulation of the Soil-Structure-Interaction (SSI) are classified into two main categories: The direct method and the substructure method.

In the direct method, both the structure and a bounded zone of soil are modelled [5], usually by the Finite Element Method (FEM). This method requires the input of motion at the external nodes of the soil and special absorbing boundaries are needed to ensure that outgoing waves will not reflect at the boundaries. There are mainly two types of absorbing boundaries: rigorous [6,7] and approximate boundaries

* Corresponding author.
E-mail address: p.a.korswageneguren@tudelft.nl (P.A. Korswagen).

https://doi.org/10.1016/j.engstruct.2021.112847
Received 3 March 2021; Received in revised form 21 June 2021; Accepted 10 July 2021
Available online 24 July 2021

[8,9,10]. This type of analysis can take into account the linear or nonlinear behaviour of the soil and the structure, as well as the heterogeneities, but can become computationally expensive, since the mesh needs to be small enough to capture the transmission of the high frequency waves.

In the case of sub-structure methods, the entire soil-structure system is subdivided into two subsystems: the superstructure, that can also include a portion of non-linear soil around the foundation, and the substructure, consisting of the unbounded soil [11]. The two subsystems can be solved with whatever approach is best appropriate for each type of model, usually FEM or Boundary-Element-Method (BEM) [12] are used for the substructure, while FEM is used for the superstructure, where also the impedance functions determined by the analysis or the substructure are included [13,14,11]. The sub-structuring method has more practical uses in engineering problems since it produces accurate results and requires a lower computational effort in comparison to the direct method. However, due to the required superposition, a linear material behaviour is usually assumed, though a few steps have been made for the inclusion of the nonlinear behaviour of the soil [4]. In recent years, a third class has emerged for the numerical modelling of the SSI, which combines characteristics of the direct and sub-structure methods and is therefore called a hybrid method. For a review on this method the reader is referred to the consistent infinitesimal finite element cell method (CIFECM) [15] and the macro-element method developed by Cremer et al. [16,17].

Codes and guidelines offer a streamlined approach where the potential dampening or amplification of the underlying soil is considered by offering ground-level pseudo acceleration or displacement spectra for a variety of seismic inputs [18,19,20]. This convenience however, is a tradeoff where the reaction of the soil as a result of the behaviour of the structure is neglected, and where specific soil information is generalised. Nonetheless, micro-zonation maps are available for some seismic regions, where soil data is included at higher resolutions [21], making the provided spectra more accurate. Incidentally, when vibration sources are located on the surface, such as vibrations originating from trains or pile-driving, it is sensible to employ a dampening law that considers geometric and material dampening or attenuation due to the soil, to determine the amplitude of the vibration at the location of the structure [22,23]. More complex models can also establish the shift or amplification of the frequency content of the vibration when it arrives at the structure [24]. Guidelines [25] can then set vibrations limits that if met, make it unnecessary to model the structure.

In many cases, the safety or damage state of the structures against vibrations can be judged by evaluating their capacity, and simple models can be sufficient for this purpose. However, when such an approximation of damage through empirical estimations is insufficient, non-linear models of the structures are required for a more accurate, quantitative analysis of damage. These models allow the inclusion of the strength and toughness of the material so as to assess their behaviour past their elastic regime. Ductile materials, such as steel, may deform permanently, and brittle or quasi-brittle materials, such as concrete or masonry, may develop cracks under tension; these can be quantified as damage. In fact, cracks and deformations are usually reported as the most common expressions of damage due to vibrations [26,27]. This type of damage has proven to be sensitive to the loading characteristics [28], especially when minor damage is contemplated [29,30]. Consequently, the assessment of minor or light damage, in this context identified as damage state one (DS1) [31], requires the use of complex models so as to include as many relevant effects as possible. These models can be elaborated using the finite element method [32,33], where both the structure and the soil are depicted using small cells or elements that can simulate the strain or stress of the various materials in the model and its development during a vibration time series. Yet, complex models also require more parameters, modelling expertise and computational resources [18,34].

There are several effects presumed to influence the light damage of structures which are sensibly omitted when assessing the ultimate capacity of structures. These comprise: the deformation of the soil under the structure, leading to bending or longitudinal tension stresses on the foundation; the time shift between the arrival of vibrations on one side of the foundation and the other; and, the rocking effects caused by vibrations [35,36]. Other effects such as the intensity of the vibrations at the structures, their directions, and their frequencies, are usually well captured by even the simplest models; while the dynamic interaction of soil and structure are also well represented by the finite element models. In order to model all the aforementioned effects, key to the correct evaluation of light damage, a large and complete model of the structure and soil system is thus necessary. Yet, the non-linear effects required for the assessment of damage, make the results of such a model dependent on the input parameters and (geometrical) properties of the structures, meaning that the model needs to be re-evaluated for every change in the parameters, making its use unfeasible due to the associated computational requirements.

The methodology presented in this paper was born out of the need to evaluate the structural response of masonry façades with different geometric and material properties, in areas with different soil profiles and where light seismic events have occurred. This is especially relevant in the province of Groningen in the north of the Netherlands, where recent events have been linked to the (light) damage of the prevalent, unreinforced masonry structures [37,38], which in turn have led to economical losses and societal unrest [39,40]. Given the number of façades, soil profiles and other loading characteristics (such as initial settlements), it was unfeasible to run simulations using the direct method for the SSI due to its large computational requirements. It was therefore decided to follow a sub-structuring approach, curated and modified to fit the software available for the numerical analyses, thus fulfilling two main objectives: to evaluate how soil layers with different properties influence the wave propagation of a signal from a deep source to the soil surface, and to assess the damage exerted on the masonry façades by the aforementioned signal, taking into account the SSI and other necessary boundary and loading conditions. A methodology was therefore developed to satisfy these objectives, while minimising the computational effort and obstacles encountered during the modelling of the soil-structure system, as is further discussed herein. The soil-structure system is subdivided into three subsystems: a model of the far-field soil (the deep model), a model of the near-field soil (the shallow model), and a model of the structure and its foundation (the non-linear decoupled model) supported on equivalent springs and dashpots. Appropriate boundary conditions are selected for the case of the soil models, so that outward waves are absorbed in the boundaries, where necessary. This decoupling of the structural non-linear finite element model from the soil model, allows the study of extensive variations of the structure, such as different material models and parameters or differing geometries. These variations are essential when assessing a wide range of structures or performing probabilistic estimations of light damage.

2. Sub-structuring methodology

As mentioned, this method comprises three sub-models: a far-field soil model (deep model), a near-field soil model (shallow model), and a super-structure model (non-linear decoupled model), that includes also the foundation and its impedance. In the latter model, the effects of the soil and the interaction between the structure and the soil are captured in springs (k_i) and dampers (c_i) with horizontal and vertical properties varied along the lateral and bottom edges of the foundation of the structure, see Fig. 1. The input, an acceleration time series representing the vibration, is modified using factors and time-shift scalars, and applied at these discrete points along the foundation. The calibration of the springs, dampers, factors, and scalars follows from the deep and shallow soil models. First, the far-field soil is represented as a 2D,

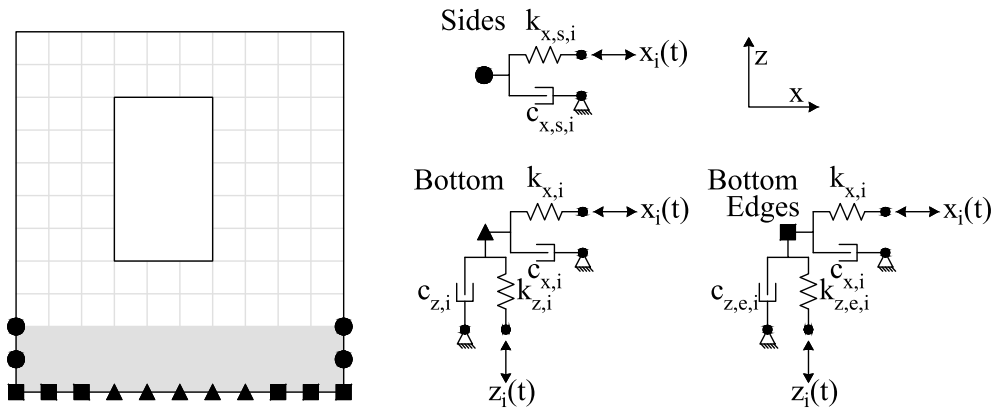

Fig. 1. Scheme of a finite element model (of a wall with a window opening) with discrete dampers and springs applied on the nodes of its foundation. Three types of nodes are discernible based on their restraint: horizontal-only (circle), horizontal-and-vertical at the edges (square), and horizontal-and-vertical at the centre (triangle). The node-dependent excitation, x(t) and z(t), is applied only at the spring end.

plane-strain model, used to mimic the propagation of the vibration through the soil from the source to the location of the structure. Then, the near-field soil model, set within the space of the far-field model and including a simplified, linear-elastic model of the structure, is employed to monitor, in higher detail, the wave propagation on the top layers and the SSI observed around the foundation of the linear structure. This second model, referred to as 'shallow model', is set to replicate on all its boundaries the vibrations generated by the far-field model at these locations (nodes). Finally, the structural model, also labelled 'the decoupled structural model', is a plane stress model that incorporates, through its boundary conditions, the soil-structure interaction observed in the near-field model. This third model is also non-linear; it includes smeared cracking in order to calculate damage. This sub-structuring approach is presented in Fig. 2 and discussed in detail in the following sections. All

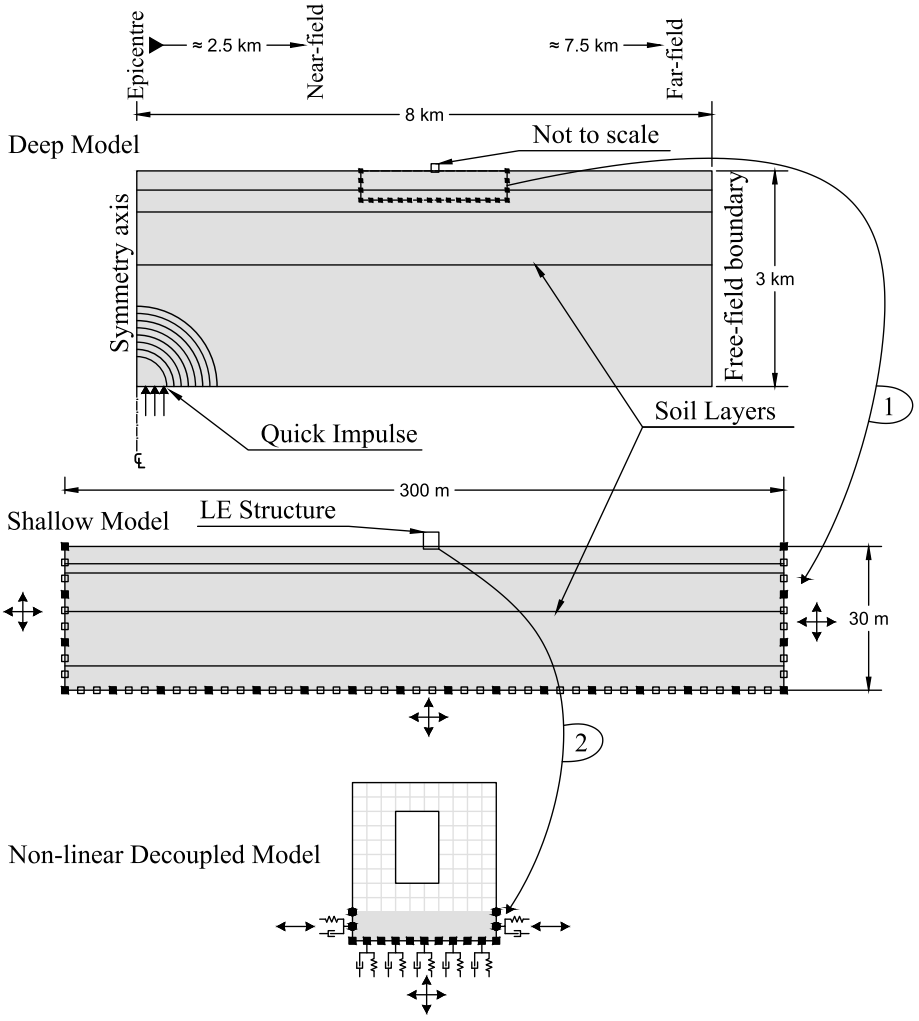

Fig. 2. Three-tiered approach with an overview of the three model steps. The mesh and soil layer divisions are for illustration purposes only.

the models used as examples were elaborated in 2D, in either plane-strain or plane-stress configurations, and using the software Diana FEA.

2.1. Far-field, deep soil model

The goal of the far-field model was to replicate the motion at the surface produced by a disturbance at a depth of 3 km. The motion was to include all the intricacies caused by reflection and refraction of the travelling waves at the boundaries of the various soil layers and by the delays caused by the difference in speed between compression and shear waves. The depth of 3 km was chosen because it corresponds to the depth of the stiff salt layer that contains the liquified gas and around which most hypocentres have been recorded [41]. The 8-node quadrilateral plane-strain elements were sized such that they would be capable of transmitting waves in the frequency range of 0–10 Hz. This is the frequency range of interest for analysing structural response and damage [42]; the element size is thus smaller than the half of the ratio between the shearwave speed of the soil and the maximum frequency of 10 Hz [34]. Moreover, the model was excited by a uniform vertical displacement at the bottom left corner over a length of 500 m. This uniform displacement of the edge nodes in the model took the shape of a pulse with a duration of 0.1 s thus including the desired frequency range as depicted in Fig. 3. This is a simplification of the mechanics of fault slipping causing shallow earthquakes, yet capable of generating a disturbance in the deep soil that, especially in a two-dimensional model, propagates to the surface in the same manner as a more detailed fault-slip event would. Ultimately, the generated motion at the surface is remarkably similar to that of actual ground motion records (see later Fig. 5) and is more than adequate for the purpose of this study. Furthermore, the two-dimensional, half-space far-field model was made symmetric around the vertical axis at the epicentre and was equipped with a non-reflective boundary at the opposite end, beyond the area of interest, to simulate the fact that travelling waves continued through the medium and did not return; as its name suggests, a non-reflective boundary ensures that waves do not reflect at the boundary and are thus absorbed by the boundary elements. These consist of boundary surface elements (BSE), that include the respective mass and stiffness of the far-field, and of interface elements that connect the BSE with the soil through dampers, resulting in a critical combination of mass, springs and dampers in the FE analysis program [52]. It is important to note that the soil model is linear-elastic as the small deformations being investigated are assumed not to require modelling of the soil's non-linear behaviour; consequently, the impulse and deformations presented can be scaled arbitrarily. Table 1 presents an example of a soil profile [43] and the corresponding dimensions of the model's elements.

Fig. 4 shows a few impressions of the travelling waves where the reflections at the soil layers can be observed. The waves become more complex as they reach the surface with reflections and refractions, and geometric and material damping (1% of proportional Rayleigh damping was assigned to the soil based on the two main modes), altering the deformations of the soil, especially at surface. Two locations of interest were defined at the surface: the first, approximately 2.5 km away from the epicentre was to represent the motion typical of earthquakes recorded 'near' the epicentre, characteristic of short significant durations, few cycles of high frequencies and higher amplitudes; while the farther location, at about 7.5 km from the epicentre, should resemble records with a longer significant duration and a higher number of cycles with low frequencies at a damped amplitude. The motion at these locations was compared to two recent natural motions. The first, corresponding to the earthquake of Zeerijp of January 8th, 2018 recorded at the Garsthuizen (2.6 km) and Appingedam (7.7 km) ground surface stations with a magnitude of 3.4 and a maximum recorded PGA of 0.11 g; and the second, of Westerwijtwerd of May 22nd, 2019 recorded at the Stedum (3.2 km) and Hoeksmeer (9.7 km) stations with a magnitude of 3.4 and a maximum recorded PGA of 0.046 g. This data was obtained from the database of the Royal Dutch Meteorological Institute (KNMI) [44]. The maximum rotated horizontal components of these 'near' and 'far' stations are compared to the two locations obtained from the model in Fig. 5.

The velocity and acceleration time series output from the deep model cannot be recognised as being synthetic when compared to the natural motions since many characteristics of the natural records are recreated in the artificial record. Fig. 5a shows that all three motions display a prominent first cycle (a.k.a. pulse) for the 'near' type of motion, while Fig. 5b shows that all three motions have a more uniform time series for the 'far' location. The more immediate release of energy of the near records can also be compared in the graphs displaying the Arias intensity, which can be used to give an indication of the significant duration of the records; here, the far records sport a much more gradual release of the energy contained in the motions. Similarly, while the far recordings have a higher content of low frequency cycles between 2 and 4 Hz, all near recordings additionally display a frequency peak between 5 and 8 Hz. Finally, the pseudo acceleration spectra, compared also to a general spectrum provided by the Dutch guideline (NPR) [18], shows that the code spectrum seems to underestimate the amplification caused by the records for the short periods but overestimates the amplification

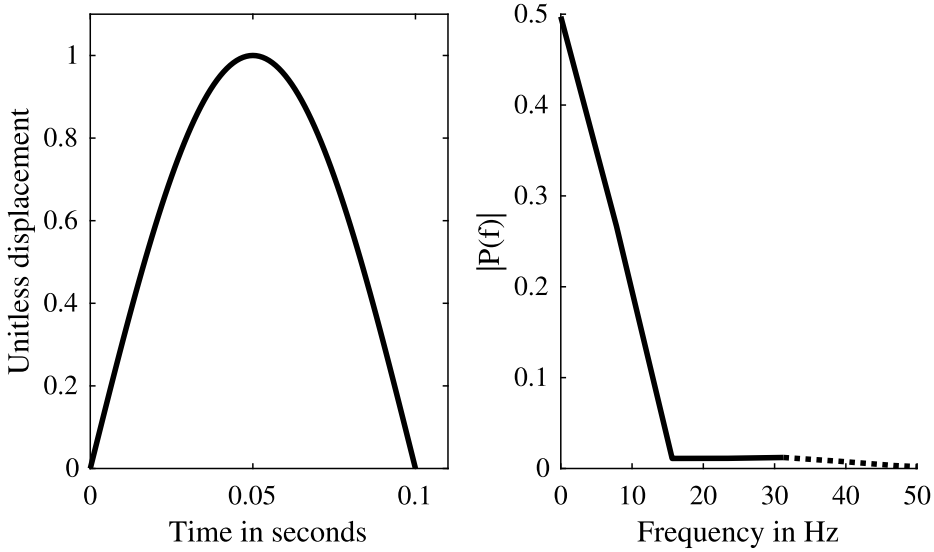

Fig. 3. Left, sine-shape impulse applied at the bottom left (500 m) of the deep model. Right, Fast-Fourier-Transform of the pulse showing frequency content.

Table 1
Soil profile for the example model adapted from soil profiles F6 and F7 in [43].

Layer	Depth	Stiffness	Poisson's Ratio	Density	Shearwave velocity	Mesh size
Silty Sand	0–9 m	94 MPa	0.30	1700 kg/m^3	145.6 m/s	2.5 × 2.5 m
Clay	9–18 m	114 MPa	0.45		152.1 m/s	
Silty Sand	18–30 m	394 MPa	0.35	2000 kg/m^3	270.0 m/s	
–	30–100 m	450 MPa	0.30		294.2 m/s	10 × 10 m
	100–500 m	550 MPa			325.2 m/s	15 × 15 m
	500–850 m	1,513 MPa	0.25		550 m/s	20 × 20 m
Base of the North Sea Group	850–2000 m	14,000 MPa	0.16	2170 kg/m^3	1666.8 m/s	25 × 25 m
	2000–3000 m					40 × 40 m

Table 2
Partial soil profile for an example 'poor soil'.

Layer	Depth	Stiffness	Poisson's Ratio	Density	Shearwave velocity	Mesh size
Sand	0–1 m	26 MPa	0.30	2000 kg/m^3	70.7 m/s	2.5 × 2.5 m
Peat	1–3 m	23 MPa	0.45	1200 kg/m^3	81.6 m/s	
Clay	3–13 m	35 MPa		1600 kg/m^3	86.6 m/s	
Sand	13–22 m	208 MPa	0.30	2000 kg/m^3	200 m/s	10 × 10 m
–	22–30 m	450 MPa			294.2 m/s	15 × 15 m

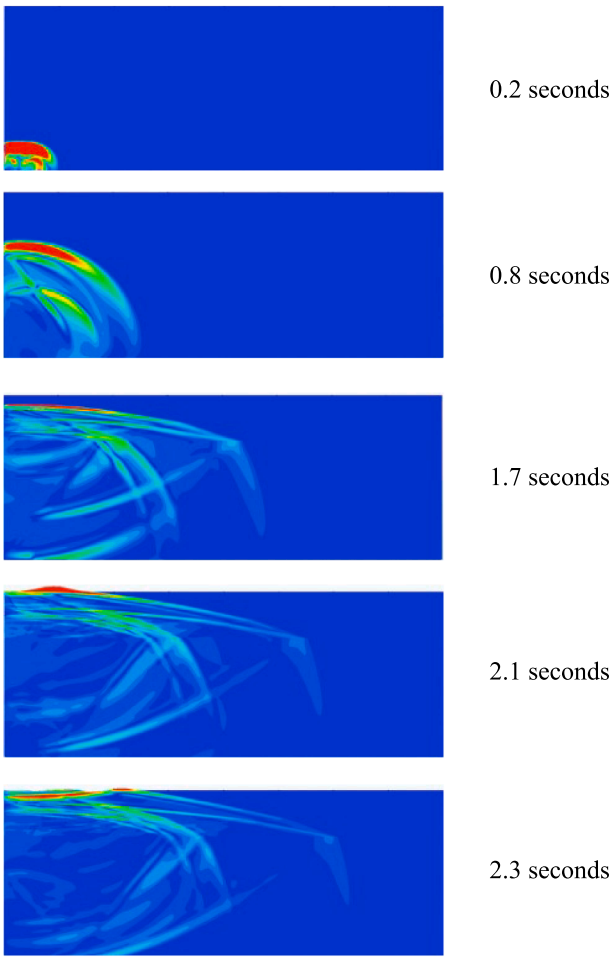

Fig. 4. Magnified view of the progression of deformation waves through the deep soil model.

for the long periods; again, the model is not identifiable as a synthetic record. Note that the vertical motion was also analysed but is not illustrated here for brevity as the comparison is similar to that of the horizontal components.

Just as the two selected natural motions cannot be considered to be fully representative of the potential motions in the region, the example soil profile presented here is but one of the potential soil variations that can be considered in the model. Changes in the soil layers, especially in the upper layers, will lead to different motion images; the soil profile presented here was heterogeneous in depth but homogeneous along the 8 km. This is not fully representative of real soil profiles, but was adopted to be as similar to profiles found around the stations where the natural motions were recorded while remaining relatively simple to model. In sum, the far-field model served the purpose of replicating the motions from real earthquakes with sufficient accuracy.

2.2. *Near-field, shallow soil model*

The mesh size of the far-field model is not capable of resolving the motion throughout the foundation of a structure. But, reducing the mesh size of the far-field model would make it unfeasible to be run in conventional computer equipment; therefore, a near-field model, placed around the location of interest, is used to locally increase the resolution while also providing the opportunity to specify more detailed soil layer properties. Moreover, the far-field model does not incorporate the structure, while the near-field model is configured to include the structure under the premise that its weight and stiffness will affect the behaviour of the neighbouring soil (soil-structure interaction). In this model, the geometry of the structure, and to some extend also the upper soil layers, can be changed without needing to redo the computationally-expensive far-field model.

Unlike the far-field model however, where only the right boundary was setup to be non-reflective, all the soil boundaries in the near-field model were made non-reflective. Additionally, the motion of all the nodes at the boundaries was enforced to mimic the motion of the respective nodes in the far-field model. A python script was written to take the output of the far-field model in terms of horizontal and vertical displacement time series and place it as the input to the boundary nodes of the near-field model. The input for nodes that do not exist in the far-field model, because of mesh size variations for instance, would need to be interpolated between the neighbouring nodes. The near-field model could be located anywhere along the surface of the far-field model; in Fig. 2, the shallow model appears in the middle.

The resulting motion at the surface of the near-field model was compared to the same locations in the far-field model for various points along the surface; the differences were virtually undetectable, meaning that a good transfer takes place between the models. Only at the point where the structure was located could differences be observed; this is due to the presence of the structure which did not appear in the far-field model. Fig. 6 shows how the travelling waves are flattened as they pass the structure; the structure does not only move horizontally, but also rocks and displaces vertically. Moreover, the motion of the soil causes bending and elongation of its foundation; these are minimal and cannot be observed at the scale of Fig. 6, but may be important contributors to

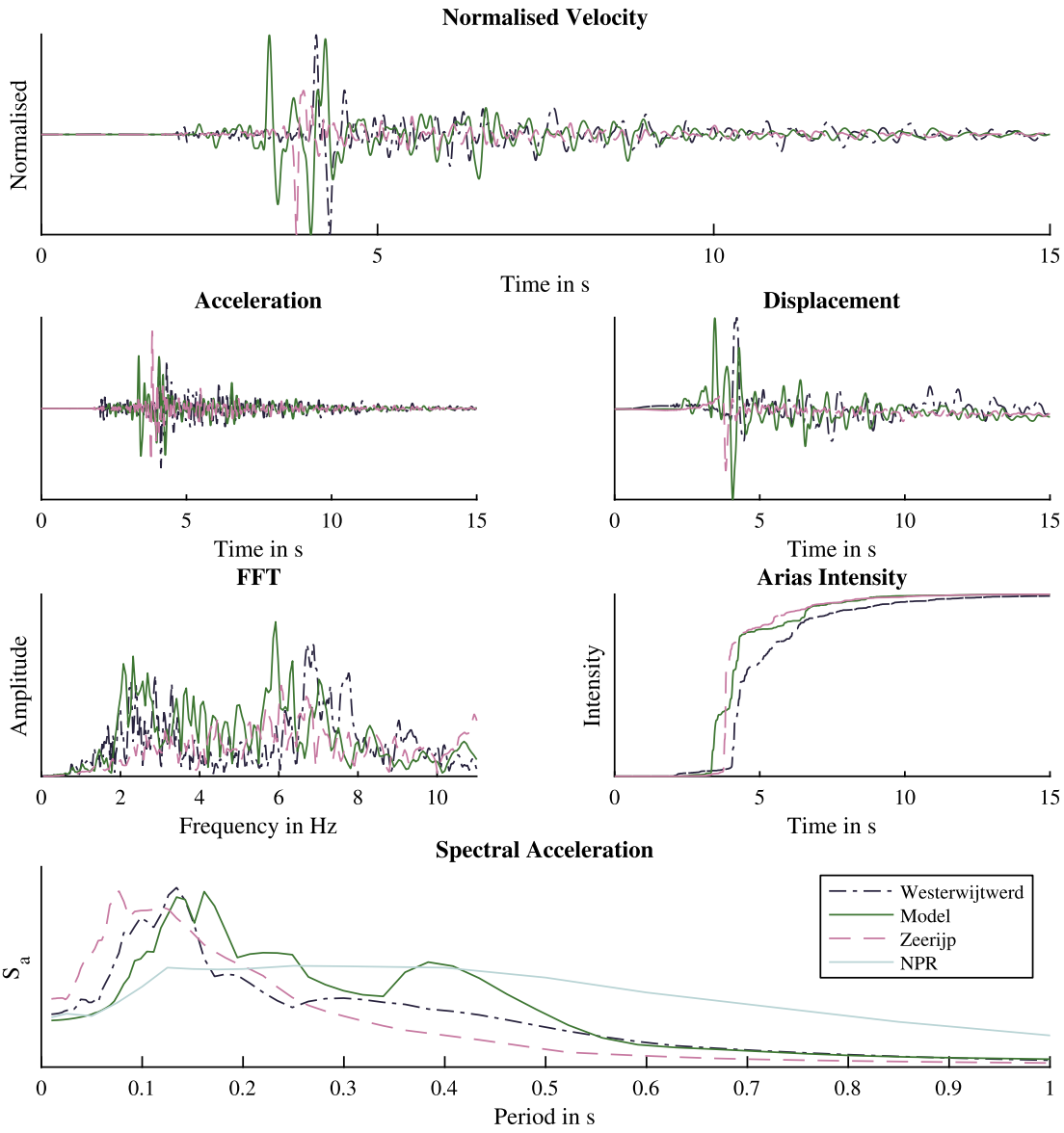

Fig. 5a. Horizontal motion at the 'near' location for the model in comparison with two recorded natural events. Values are normalised to the Peak Ground Velocity.

the light damage of the structure. Consequently, the motion of all the nodes around the foundation is later transferred to the decoupled, non-linear model of the structure.

The structure in the near-field model is linear-elastic, yet its inclusion is not without challenges: the plane-strain model of the soil represents a unitary width of soil which in turn can be observed as an infinitely thick model. This is reasonable for modelling the ground but does not apply well to a structure which has distinctively finite thickness. This is the incompatibility of plane-strain against plane-stress. The structure needs to be represented with a density and stiffness which are compatible with the soil model and the later decoupled model; this approach with 'correction factors' is viable for the linear approximation of the structure but is not possible for its non-linear counterpart. This is a key reason why the decoupled (non-linear) model is preferred, as the interaction with the soil is captured in the springs and dashpots and no correction factors need to be employed. Consequently, in the near-field soil model, the 2D façade of interest of the structure appears with reduced density and stiffness at a ratio of its real thickness over the unitary thickness of the plane-strain soil model. This approach also assumes that the effect of the foundation of the structure is continuous in the plane perpendicular to the model; this approximation is valid if walls and foundations perpendicular to the façade are present. Furthermore, models with and without the structure demonstrated that the effect of the presence of the structure was negligible when observing the behaviour of the soil around it; hence, the inclusion of the structure in the soil model has, as its greatest advantage, the derivation of the motion of the nodes around the foundation, which includes the soil-structure interaction. This displacement time-series is later used as input at the foundation of the decoupled structural model.

2.3. Decoupled model

The aim of the decoupled model, as depicted in Fig. 1, is to work independently of the soil models (Fig. 2) and allow for a non-linear representation of the structure on the soil. To simulate the presence of the soil, the detailed method summarised by NEHRP [45], based on the partially empirical equations of Gazetas [46] and comprising the definition of springs and dampers around the foundation, is adopted. The results obtained with this method were compared to the behaviour of the linear structure on the near-field soil model as is discussed later on. The influence of the soil is captured in distributed horizontal springs attached to the sides of the foundation ($k_{x,s,i}$), while the bottom of the

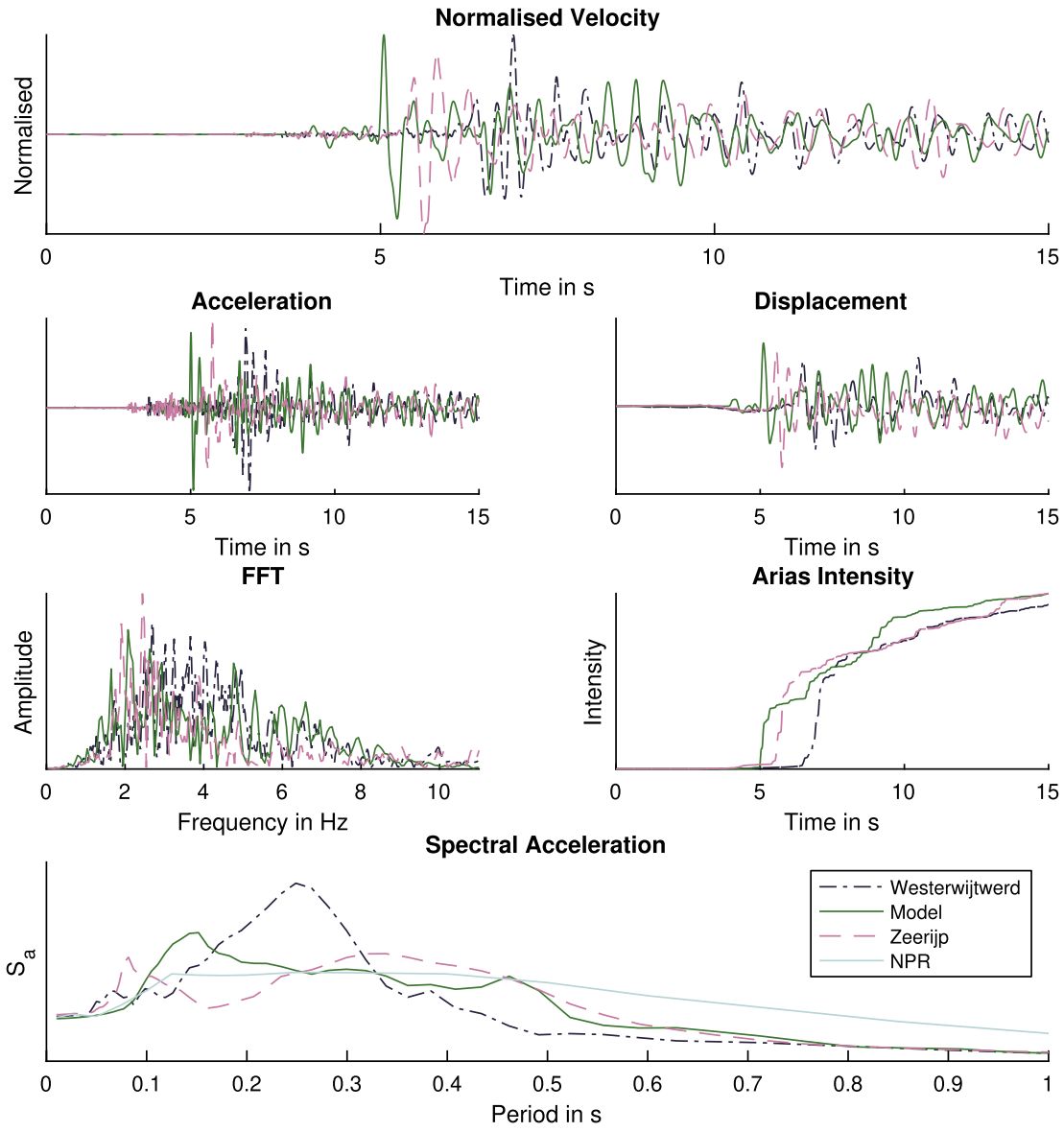

Fig. 5b. Horizontal motion at the 'far' location for the model in comparison with two recorded natural events. Values are normalised to the Peak Ground Velocity.

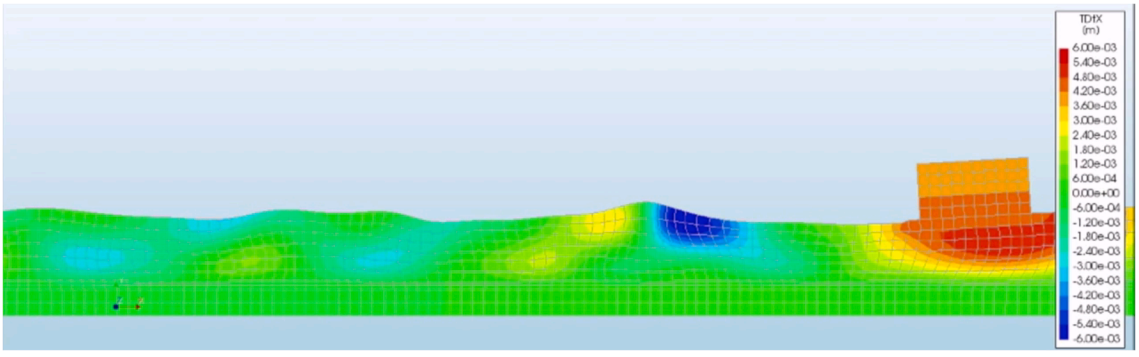

Fig. 6. Deformation of the shallow model showing rocking of the structure (rectangle on the right). Colouring refers to the horizontal displacements, and deformations are greatly exaggerated for illustration purposes.

foundation is restrained with both horizontal ($k_{x,i}$) and vertical ($k_{z,i}$) distributed springs; the edges of the bottom of the foundation are subjected to modified spring stiffness ($k_{z,e,i}$). The damping coefficient (c_i) of the dashpot elements is analogous. The definition of these parameters is not altered from the implementation of NEHRP [45] and is too extensive to be reproduced here, so only an overview and brief example are provided herein. Note that this method is meant for shallow foundations such as those present in the older masonry structures considered in this

study; structures with pile foundations will behave differently and are the topic of a future study. First, the soil is characterised by its Poisson's ratio, its shear modulus (G) and its mean shearwave velocity (V) directly underneath the foundation over a depth equal to the square root of the area of the foundation, or, when rocking effects are considered, the fourth root of the moment of inertia of the foundation [45]. Then, for the main vibration period of the structure (T), the springs and dashpots can be computed based on the width and length of the shallow foundation, B and L, respectively. Furthermore, the distance where the modified stiffness and damping at the edges of the foundation are applied, was calibrated against the near-field model with the result that assigning each corner 20% of the length delivered the best results. Finally, under the assumption that the Poisson ratio of the soil is 0.35, that the depth of the shallow foundation of the structures considered is 0.6 m, and that the length of the foundation is around five times the width (L = 5·B), the parameters can be approximated to:

$$k_{z,i} = \frac{G\cdot\left(1.8+\frac{0.29}{B^{2/3}}\right)\cdot(B+0.072)\cdot\left(0.77\cdot T^2\cdot V^2+5.5\cdot B^2\right)}{\left(0.77\cdot T^2\cdot V^2+9.9\cdot B^2\right)\cdot B^2} \quad (1)$$

$$c_{z,i} = \frac{G\cdot(2\cdot B+1.44)}{V\cdot B} \quad (2)$$

$$k_{x,i} = \frac{1.4\cdot G}{B} \quad (3)$$

$$c_{x,i} = \frac{G\cdot(B+1.7)\cdot\left(1+\frac{0.16}{B^{1/2}}\right)\left(1+\frac{0.16}{B^{4/5}}\right)}{V\cdot B} \quad (4)$$

Note that because of the assumptions required to simplify these equations, they are not unitless, but are expressed instead using SI units (kg, m, s). The goal of this simplification is to be able to draw some observations regarding the definition of the parameters. First, the equivalent vertical stiffness of the soil (Eq. (1)), depends on all the parameters. Both the static and dynamic influence of the soil is included as G and V, and the static and dynamic properties of the structure are present in B and T. For the horizontal stiffness (Eq. (3)), only the static properties of soil and structure, G and B, respectively, seem relevant. Similarly, both horizontal and vertical damping is not dependent on the dynamic properties of the structure (T), but do involve the other parameters. Moreover, under these assumptions, the ratio $k_{x,s,i}/k_{x,i}$ is around 1.3, while the ratio $c_{x,s,i}/c_{x,i}$ is around 0.6. Both of these ratios remain only dependent on the geometry of the foundation and present reasonable values as the horizontal stiffness on the side, where the soil is pressed (passive pressure), is larger than at the bottom; and damping on the side, closer to the ground surface, diminishes. Likewise, the ratio $c_{z,e,i}/c_{z,i}$ is around 0.35, and the ratio $k_{z,e,i}/k_{z,i}$ is around 10. The significantly higher vertical stiffness towards the edges of the foundation is to counteract the rocking potential of the structure.

The stiffness and damping parameters were introduced to the decoupled model around the foundation. The distributed stiffness was assigned as an interface, while the damping parameter was included in a separate interface layer [18]. Three adjustments to the method of NEHRP [45] were developed: First, the end length ratio (R_e) was determined to be most suited at a value of 0.4, or 20% for each edge of the foundation. Second, the springs were made non-linear, assuming no-tension behaviour, so that only compression forces with linear stiffness could develop while gapping occurs in tension, which represents the interface between foundation and soil. Third, the displacement time histories, x(t) and z(t), were applied at the opposite end of the "springs", as illustrated in Fig. 1. This produced the best results but also enabled the inclusion of multi-phased analyses; for example, a settlement profile could be applied that deformed the support of the foundation. Because the springs were configured not to resist tension, the structure was not forced to deform but allowed to settle naturally. Then, a displacement time history could be applied on the soil end to mimic the effect of a vibration after potential, pre-existing settlement damage.

The displacement time-histories were applied as recorded from the shallow model; that means, different points throughout the foundation were subjected to slightly different time histories. To generalise the relationship between the nodes such that arbitrary natural motion records could be applied, an amplitude factor (α_d) and a time-shift parameter (t_s) were determined from the time series recorded from the near-field model for each soil profile. In other words, the original record is scaled differently for distinct points on the foundation and is affected by a small time delay for each distinct point. These two parameters are linearly dependent on the distance measured from one corner of the foundation such that the input for each node on the foundation can be determined using Eq. (5), where $x_0(t)$ is the original record or the record at the corner closest to the source. The values in metres for α_d and t_s can be found in Table 3 and Table 4, respectively, for both x(t) and z(t). The original record will be unmodified for x = 0 and will be most affected for x = L by α_d·L and t_s·L.

$$x(t) = (1+\alpha_d\langle x\rangle)\cdot x_0(t-t_s\langle x\rangle) \quad (5)$$

A positive value of α_d leads to an amplification of the record while a positive value of t_s means that the peak of the record arrives later at the corner of the foundation farthest from the source. This directionality is irrelevant in most cases, but is important when looking into the physical significance of the parameters. Observing the values in Table 3 reveals that the horizontal component of a record is amplified on the farthest end when the soil is relatively good, but is damped when the soil is poor, independent of the distance to the epicentre. Conversely, the vertical component seems to be amplified irrespective of the soil for the near cases, but is damped for the far locations. The time-shift parameter in Table 4 is, of course, always positive as it would not be possible for the peak to arrive earlier on the farthest corner of the foundation. Yet, differences can be observed between the horizontal and vertical components and the good and poor soil profiles (Table 1 and Table 2). Mainly, the far locations display a greater difference between the arrival time of the record between one end of the foundation and the other, with this difference being slightly larger for the good soil profile. Reversely, at the near locations, the good soil profile displays a smaller time lag.

While the displacement time histories between the surface of the far-field model and the shallow model, and between the top of the wall in the near-field model and the model supported by springs, are virtually indistinguishable, subjecting the wall on the near-field model and on the one supported by springs to a dead load, does show some slight differences; Fig. 7 compares these two walls. Here it can be observed that the wall on soil sinks more evenly while the one on springs, due to the stiffer springs at the corners, sags more towards the middle.

In sum, displacements are matched between the deep, shallow and decoupled models so as to ensure the validity of the transitions between the models. This guarantees proper calibration values for equivalent stiffness, damping, amplification, and time-shift values at the nodes of the bases of the decoupled models, and means that non-linear decoupled models can be run behaving as if a large soil block was underneath them and as if the seismic input signal was not applied directly at its base, but at the base of a large soil block; the latter producing a time-shift between the velocities applied at each of the nodes. These amplitude and time shift parameters also illustrate the (un)importance of these effects for other types of models in other studies.

Table 3
Amplitude modifier factor.

α_d (m^{-1})	Horizontal Component		Vertical Component	
	Near	Far	Near	Far
Soil A (Table 1)	1.2E-03	3.5E-04	2.5E-04	−5.9E-04
Soil B (Table 2)	−2.0E-04	−1.3E-05	2.6E-04	−6.2E-04

Table 4
Time shift parameter.

t_s (s·m^{-1})	Horizontal Component		Vertical Component	
	Near	Far	Near	Far
Soil A (Table 1)	7.6E-05	3.5E-04	5.5E-05	5.1E-04
Soil B (Table 2)	9.9E-05	3.0E-04	7.0E-05	4.7E-04

3. Comparison between models with and without soil-structure interaction

To assess the influence of the soil-structure interaction and input modification of the proposed method, three sets of non-linear models were run. The first set consisted of models with a fixed base to which a natural motion record was applied. The second set comprised models with springs and dashpots and a location-dependent input signal such as described in the previous section. Finally, the third set included the application of a ground settlement case before the natural motion is applied to the models (pre-settlement) and was otherwise identical to the second set. The material model and parameters for all the models were the same and followed an extensive calibration campaign, where full-scale experimental tests were replicated with non-linear finite element models capable of simulating the cracking behaviour of masonry [47]. An orthotropic total-strain based masonry model (also called Engineering Masonry Model - EMM in Diana FEA) was selected as constitutive model [48,49,50]. This model includes different values of inelastic and elastic properties for the two main directions: the local 'x' parallel to bed-joints and local 'y' aligned with the head-joints. The in-plane crack directions are four: two of them are located along the joints' axes and the other two are diagonal, taking into account the masonry pattern by a parameter (predefined angle for diagonal cracking). As failure mechanisms, the material model includes tensile cracking with softening and secant nonlinear unloading/reloading behaviour, Coulomb friction with cohesion softening and elastic unloading/reloading, and compression crushing (in both horizontal and vertical directions) with mixed secant/elastic unloading and reloading behaviour. Multiple options for the head-joint failure can be considered in the material model. For the calibration model, the "friction based" option was selected. In this case, the tensile strength of the head-joint is calculated from the friction shear-stress in the bed-joint, though a minimum value of tensile strength in the head-joint must be provided. For robustness and simplicity, the Poisson's ratio of the model was set to zero; this has an influence on the elastic behaviour of the model, but since the focus of this study is on the non-linear behaviour (cracking) of the material, where Poisson's ratio effectively diminishes to zero during softening, and for which the orthotropic EMM does link the two directions as discussed above, the assumption has been considered valid. The values and parameters employed are collected in Table 5.

Two types of 2D-structures were modelled: a simple wall with an asymmetrical window opening, and a complex façade with multiple openings; these are illustrated in Fig. 8 and additional details about the models' geometries can be found in contemporary studies [29,30]. Fig. 8 also presents the final crack pattern for the third set of models; the intensity of the damage pattern is evaluated using the parameter Ψ which considers the width, number and length of the cracks so as to express damage in a single scalar [30]. Cracks around 0.1 mm in width are reflected in a value around $\Psi = 1$ and correspond to visible light damage, while a value of $\Psi = 2$ is linked to a greater number or to much wider cracks of up to 1 mm. This parameter can then be used to determine the progression of damage but also to assess the influence of the soil-equivalent foundation. The seismic motion applied corresponds to the natural motion recorded during the earthquake of Zeerijp of January of 2018 scaled to a horizontal PGV of 20 and 32 mm/s; the latter value corresponds roughly to 0.1 g PGA [37]. For the soil-structure interaction, the soil described in Table 1 was used. Table 6 offers a comparison between the three approaches and shows that including the potential interaction with the soil and the slightly altered input on each foundation node to reflect the deformation of the foundation caused by the natural motion, leads to an increase in measurable damage. For a PGV of 32 mm/s this increase is about 12%; however, for the lower value of 20 mm/s, the model without SSI didn't present any damage while the inclusion of the adjustments presented herein, did lead to a small value of damage. These small yet clear increases are paramount when assessing light damage [51]. In comparison to the simpler wall, the larger façade displayed a slightly larger increase in damage when SSI was considered; this is likely due to the longer foundation of the façade which allows for

Table 5
Material properties of macro-model. *(1-Tested Value, 2-Estimated Value, 3-Computed value)*.

Material Properties	Clay Masonry	
Density	1624 kg/m^3	*1*
Elastic Modulus Perpendicular to Bed-Joints	3 571 MPa	*1*
Elastic Modulus Parallel to Bed-Joints	2 497 MPa	*1*
Elastic Shear Modulus	1 500 MPa	*2*
Bed-Joint Tensile Strength	0.16 MPa	*1*
Minimum Head-Joint Tensile Strength	0.16 MPa	*2*
Tensile Fracture Energy	11.30 N/m	*3*
Vertical/Horizontal Compressive Strength	12.93 MPa	*1*
Vertical/Horizontal Compressive Fracture Energy	35 590 N/m	*1*
Friction Angle (Friction Coefficient)	0.688 rad (0.82)	*1*
Cohesion	0.17 MPa	*1*
Shear Fracture Energy	209 N/m	*1*
Head Joint Failure Option	Friction Based	
Predefined Angle for Diagonal Cracking	0.50 rad	*1*

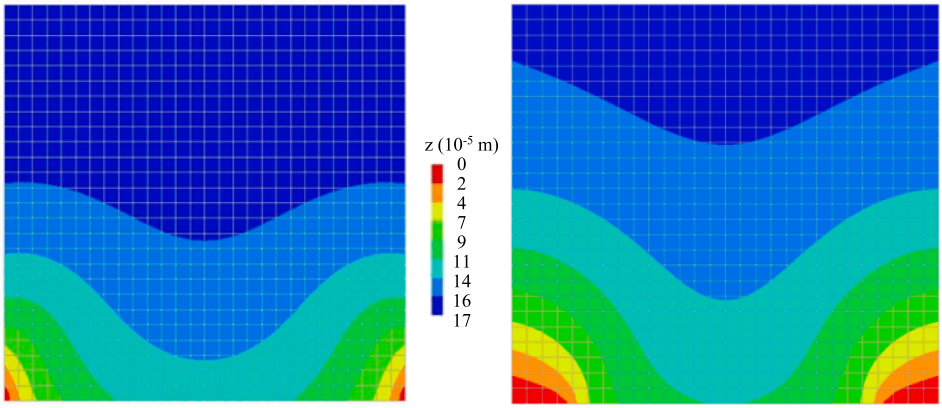

Fig. 7. Comparison for dead-load deformation between plane-strain wall on the soil model (left) and a plane-stress wall supported on springs (right). Deformation is relative to the least displaced point.

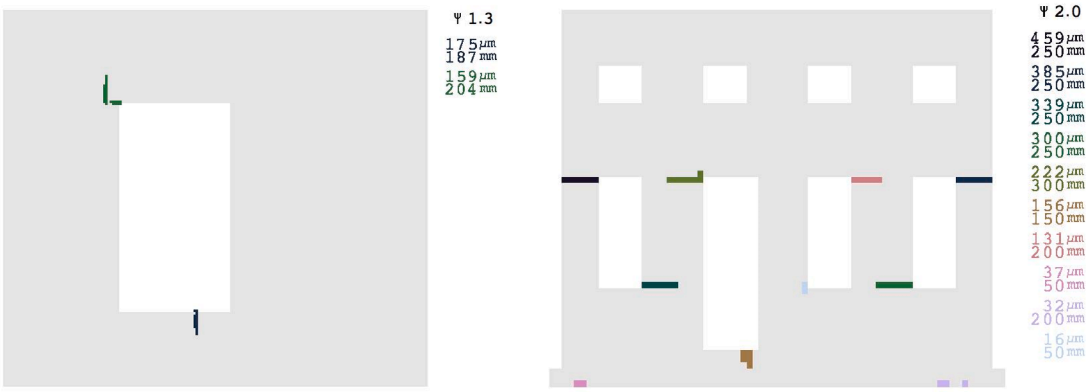

Fig. 8. Crack representation of the masonry wall and façade after settlement followed by base motion of 32 mm/s. Models supported by springs and dashpots. The damage intensity (Ψ) of the sum of cracks is calculated. Dimensions not to scale.

larger deformations when SSI is included in contrast to the zero deformations of a fixed foundation.

Moreover, the approach with a flexible support also allows for the inclusion of other ground-related actions, such as differential settlements. The existing settlement-induced damage is key in defining the result of the subsequent seismic actions [29,51]. The third set of models include a hogging-type differential settlement where one end of the foundation is allowed to sink and the other stays undeformed; the non-linear springs without tension strength ensure that the deformation is applied realistically. The settlement action is such that the wall attains a damage intensity of $\Psi_0 = 0.5$ and the façade a $\Psi_0 = 1.6$. Then, after the seismic motion is applied, the wall reaches a damage intensity 120% to 160% higher and the façade only 12% to 25% higher for the PGV values of 20 and 32 mm/s respectively. The smaller increase is attributable to the higher initial damage state of the façade. In the case of the wall, the small initial damage is detrimental to the response of the structure. In both cases, however, the light damage accumulates, highlighting the importance of considering this kind of compound damage mechanisms [27].

It must also be highlighted that these investigations have focused on the in-plane behaviour of the façades as light damage has shown to be mostly in-plane [29]. The walls and façades considered are single-wythe. The small effects studied, such as the shape of the deformation of the foundation or the time-shift between one end of the foundation and the other, are mostly relevant for the in-plane behaviour of the masonry; in this light, out-of-plane effects have been neglected.

Finally, a few comments regarding the modelling procedure are made: Firstly, phased analyses comprising gravity loads, settlements and seismic actions need to be verified at each stage to ensure that deformations are as expected. Sometimes ties overlapping the interfaces can be incorporated at the seismic stage when the settlement stage has led to large openings at the soil-structure interface. Secondly, the plane-stress nature of the decoupled model should be carefully considered in the plane-strain shallow models. Thirdly, an automatic procedure should be implemented to convert the output of the far-field and shallow models as input to the subsequent models in order to avoid tedious work.

4. Conclusions

The methodology presented herein was developed to assess the sensitive response of masonry structures and their potential damage due to light seismic events, taking into account the soil-structure-interaction in a straightforward manner. Simultaneously, the proposed methodology limits the computational burden of running the entire soil-structure system repeatedly, especially when the focus of the research is in probabilistic variations of the superstructure rather than the substructure. Moreover, the decoupling of the models helps to tackle the plane-stress and plane-strain incompatibility between structural models and soil models, while the inclusion of the foundation impedance in the structural model allows the study of combined damaging actions like differential settlements and vibrations. The methodology presented herein allows for the consideration of the effect of soil (interactions) where small variations such as the delay of arrival of vibrations between one side of the foundation and the other and the resulting rocking of the structure, or the dampening of the soil, play an important role in the resulting damage, leading to an integral approach formulated to overcome computational limitations. The methodology encompasses the usage of two large soil models to quantify the effect of the soil into damping and stiffness parameters for equivalent interfaces at the foundation of the structural models. This transfer results in parameters defining the behaviour of typical soil profiles, which can be used in FEM models with soil-structure interaction.

The example case studies presented herein showed that damage to masonry walls and façades increased approximately 15% when considering a foundation with the soil-structure interaction parameters compared against the case of a fixed foundation. Moreover, the parametrised foundation allowed also for the consideration of multi-phased analyses such as differential settlements acting before vibration loads; in the case studies, the compound loading led to an accumulation of damage. Hence, the potential of modelling multi-hazards is important when quantifying light damage. Nonetheless, the approach presented in this paper has only been qualitatively validated against natural ground motions, but has not yet been further validated against field data. A cross-validation against similar modelling approaches and techniques could also further validate the method. Moreover, the intermediate near-field model allows for non-linear modelling of the top layer of soil without having to include the non-linearity in the full soil model; this additional advantage of the method is yet to be explored alongside a more comprehensive sensitivity study of the dimensions of the near-field model and the effect of very poor soil layers under high water pressure.

Table 6
Comparison between three model approaches. The values in brackets correspond to the damage value before the motion.

			Approach 1	Approach 2	Approach 3
SSI-Base			–	**o**	**o**
Node-dependent input			–	**o**	**o**
Settlement pre-damage case (value in brackets)			–	–	**o**
Ψ	**Wall**	**20 mm/s**	0	0.65	1.1 (0.5)
		32 mm/s	0.9	1.0	1.3 (0.5)
	Façade	**20 mm/s**	0	0.5	1.8 (1.6)
		32 mm/s	0.8	0.9	2.0 (1.6)

CRediT authorship contribution statement

Michele Longo: Conceptualization, Methodology, Software, Formal analysis, Investigation, Data curation, Writing - review & editing. **Marianthi Sousamli:** Conceptualization, Methodology, Software, Formal analysis, Investigation, Writing - review & editing. **Paul A. Korswagen:** Validation, Formal analysis, Writing - original draft, Visualization. **Piet Staalduinen:** Conceptualization, Methodology, Supervision. **Jan G. Rots:** Conceptualization, Supervision, Funding acquisition.

Declaration of Competing Interest

The authors declare that they have no known competing financial interests or personal relationships that could have appeared to influence the work reported in this paper.

Acknowledgments

This work was performed partly in a related case-based study for Nationaal Coordinator Groningen (NCG), and partly included in the fundamental research into light damage mechanics of masonry structures undertaken for Nederlandse Aardolie Maatschappij (NAM). This concession is gratefully acknowledged.

References

[1] Noorlandt R, Kruiver PP, de Kleine MPE, Karaoulis M, de Lange G, di Matteo A, et al. Characterisation of ground motion recording stations in the Groningen gas field. J Seismol 2018;22:605–23. https://doi.org/10.1007/s10950-017-9725-6.
[2] Korff M. Deformations and damage to buildings adjacent to deep excavations in soft soils. COB, Delft Cluster - Deltares - publications.deltares.nl; 2009.
[3] Bird JF, Bommer JJ, Crowley H, Pinho R. Modelling liquefaction-induced building damage in earthquake loss estimation. Soil Dyn Earthquake Eng 2006;26(2006):15–30.
[4] Pitilakis, Dimitris. Soil-Structure Interaction Modeling Using Equivalent Linear Soil Behavior In The Substructure Method. PhD Thesis - Department of Civil Engineering, Aristotle University of Thessaloniki, Greece; 2006.
[5] Ghandil M, Behnamfar F. The near-field method for dynamic analysis of structures on soft soils including inelastic soil–structure interaction. Soil Dyn Earthquake Eng 2015;75(2015):1–17.
[6] Manolis GD, Beskos DE. Boundary Element Methods in Elastodynamics. Unwin Hyman, London, U.K.; 1988.
[7] Song C, Wolf JP. The scaled boundary finite-element method–alias consistent infinitesimal finite-element cell method–for elastodynamics. Comput Methods Appl Mech Eng 1997;147:329–55.
[8] Lysmer J, Kuhlemeyer RL. Finite dynamic model for infinite media. J Eng Mech Division – ASCE, 1969; 95(EM4): 859877.
[9] Clayton R, Engquist B. Absorbing boundary conditions for acoustic and elastic wave equations. Bull Seismol Soc Am 1977;67(6):1529–40.
[10] Aubry D, Modaressi H. Seismic wave propagation in soils including non-linear and pore pressure effects in Recent Advances in Earthquake Engineering and Structural Dynamics, pages 209–224. Ouest Editions/AFPS, Nantes, France; 1992.
[11] Halabian Amir M, Hesham El Naggar M. Effect of non-linear soil–structure interaction on seismic response of tall slender structures, Soil Dynamics and Earthquake Engineering 2002; 22(8): 639-658, ISSN 0267-7261, https://doi.org/10.1016/S0267-7261(02)00061-1.
[12] Karabalis DL, Mohammadi M. 3-D dynamic foundation–soil–foundation interaction on layered soil. Soil Dyn Earthquake Eng 1998;17:139–52.
[13] Zhang Xiong, Wegner J, Haddow J. Three-dimensional dynamic soil–structure interaction analysis in time. Earthquake Eng Struct Dyn 1999;28:1501–24.
[14] Wegner JL, Yao MM, Zhang X. Dynamic wave–soil–structure interaction analysis in the time domain. Computers & Structures 2005;83(27):2206–14. https://doi.org/10.1016/j.compstruc.2005.04.004. ISSN 0045-7949.
[15] Song C, Wolf JP. The scaled boundary finite element method—alias consistent infinitesimal finite element cell method—for diffusion. Int J Numer Meth Engng 1999;45:1403–31.
[16] Cremer C, Pecker A, Davenne L. Cyclic macro-element for soil–structure interaction: material and geometrical non-linearities. Int J Numer Anal Meth Geomech 2001;25:1257–84. https://doi-org.tudelft.idm.oclc.org/10.1002/nag.175.
[17] Chatzigogos CT, Pecker A, Salencon Jean. A Macro-Element for Dynamic Soil-Structure Interaction Analyses of Shallow Foundations. In: 4th International Conference on Earthquake Geotechnical Engineering June 25-28, 2007 Paper No. 1387; 2008.
[18] NEN (2018). Nederlandse Praktijkrichtlijn (NPR) 9998 - Dutch guideline of practice. NEN.
[19] EN 1998-1. Eurocode 8: Design Of Structures For Earthquake Resistance. 1st ed. Brussels: BSi; 2004.
[20] Borzi B, Calvi GM, Elnashai AS, Faccioli E, Bommer JJ. Inelastic spectra for displacement-based seismic design. Soil Dyn Earthquake Eng 2001;21(2001):47–61.
[21] Kruiver PP, van Dedem E, Romijn R, de Lange G, Korff M, Stafleu J, et al. An integrated shear-wave velocity model for the Groningen gas field, The Netherlands. Bull Earthquake Eng 2017;15:3555–80. https://doi.org/10.1007/s10518-017-0105-y.
[22] Kim DH, Lee JS. Propagation and attenuation characteristics of various ground vibrations. Soil Dynamics Earthquake Eng 2000;19(2):115–26. https://doi.org/10.1016/S0267-7261(00)00002-6.
[23] Suhairy SA. Prediction of Ground Vibration from Railways. SP Swedish National Testing and Research Institute; 2000.
[24] Hildebrand R, Keskinen E, Romero Navarrete JA. Vehicle vibrating on a soft compacting soil half-space: ground vibrations, terrain damage, and vehicle vibrations. J Terramech 2008;45(2008):121–36.
[25] SBR. Trillingsrichtlijn Deel A (2017). SBR; 2017.
[26] NAM. Trillingsschade aan gebouwen. NAM 170822-HA; 2017.
[27] Korswagen PA, Jonkman SN, Terwel K. Probabilistic assessment of structural damage from coupled multi-hazards. Structural Safety 2019;76:135–48. https://doi.org/10.1016/j.strusafe.2018.08.001. ISSN 0167-4730.
[28] Sarhosis V, Dais D, Smyrou E, Bal IE. Evaluation of modelling strategies for estimating cumulative damage on Groningen masonry buildings due to recursive induced earthquakes. Bull Earthq Eng 2019. https://doi.org/10.1007/s10518-018-00549-1.
[29] Van Staalduinen PC, Terwel K, Rots JG.. Onderzoek naar de oorzaken van bouwkundige schade in Groningen Methodologie en case studies ter duiding van de oorzaken. Delft University of Technology. Report number CM-2018-01, 11 July 2018 - Downloadable from www.NationaalCoordinatorGroningen.nl; 2018.
[30] Korswagen PA, Longo M, Meulman E, Rots JG. Crack initiation and propagation in unreinforced masonry specimens subjected to repeated in-plane loading during light damage. Bull Earthq Eng 2019. https://doi.org/10.1007/s10518-018-00553-5.
[31] de Vent I, Rots JG, van Hees RPJ. Structural Damage in Masonry - Developing diagnostic decision support. TU Delft repository.tudelft.nl; 2011.
[32] Spyrakos CC, Xu C. Seismic soil–structure interaction of massive flexible strip-foundations embedded in layered soils by hybrid BEM–FEM. Soil Dyn Earthquake Eng 2003;23(2003):383–9.
[33] Schauer M, Rodriguez GR. A coupled FEM-SBFEM approach for soil-structure-interaction analysis usi/ng non-matching meshes at the near-field far-field interface. Soil Dyn Earthquake Eng 2019;121(2019):466–79.
[34] Raaijmakers BHJ. Modellering van Constructies bij een Dynamische Excitatie via de fundering. TNO; 1994.
[35] Boffi G, Castellani A. Effects of Surface Waves on the Rotational components of earthquake motion. Proceedings of Ninth World Conference on Earthquake Engineering, 1988 Tokyo-Kyoto, Japan; 1988.
[36] Castellani A, Boffi G. Rotational components of the surface ground motion during an earthquake. Earthquake Eng Struct Dyn 1986;14:751–67.
[37] den Bezemer T, van Elk J. Special Report on the Zeerijp Earthquake – 8th January 2018. NAM; 2018.
[38] Crowley H, Pinho R, Van Elk J, Uilenreef J. Probabilistic damage assessment of buildings due to induced seismicity. Bull Earthq Eng 2018. https://doi.org/10.1007/s10518-018-0462-1.
[39] Crowley H, Pinho R, Bommer JJ. A probabilistic displacement-based vulnerability assessment procedure for earthquake loss estimation. Bulletin of Earthquake Engineering 2004;2:173–219.
[40] Crowley H, Pinho R, Cavalieri F. Report on the v6 Fragility and Consequence Models for the Groningen Field. NAM; 2019.
[41] NAM, M. Pickering, J. van Elk, D. Doornhof. An estimate of the earthquake hypocenter locations in the Groningen Gas Field. NAM; 2015.
[42] van Elk JF, Bourne SJ, Oates SJ, Bommer JJ, Pinho R, Crowley H. A Probabilistic Model to Evaluate Options for Mitigating Induced Seismic Risk. Earthquake Spectra; 2019. DOI: 10.1193/050918EQS118M.
[43] Deltares rapport 1209862-005-GEO-0004, Versie 5, bijlage F, 16 March 2015.
[44] KNMI Seismic & Acoustic Data Tools - rdsa.knmi.nl.
[45] NEHRP. Soil-Structure Interaction for Building Structures. NIST GCR 12-917-21 U. S. Department of Commerce National Institute of Standards and Technology; 2012.
[46] Gazetas G. Formulas and Charts For Impedances Of Surface and Embedded Foundations. Journal of Geotechnical Engineering 1991; 117(9), September, 1991 ©ASCE, ISSN 0733-941O/91/0O09-1363.
[47] Korswagen PA, Longo M, Rots JG. High-resolution monitoring of the initial development of cracks in experimental masonry shear walls and their reproduction in finite element models. Eng Struct 2020;211(2020).

[48] Rots JG, Nauta P, Kusters GMA, Blaauwendraad J. Smeared Crack approach and fracture localization in concrete. Heron 1985;30:No 1.
[49] Schreppers GMA, Garofano A, Messali F, Rots JG. DIANA validation report for masonry modelling. DIANA FEA report 2016-DIANA-R1601 TU Delft Structural Mechanics Report CM-2016-17; 2016, 143 pp.
[50] Rots JG, Messali F, Esposito R, Jafari S, Mariani V. Computational Modelling of Masonry with a view to Groningen induced Seismicity. 10th SAHC Structural Analysis of Historical Construction, Leuven; 2016.
[51] Korswagen P, Longo M, Meulman E, Rots JG. Experimental and Computational Study of the Influence of Pre-Damage Patterns in Unreinforced Masonry Crack Propagation Due to Induced, Repeated Earthquakes. 13th North American Masonry Conference, Utah, USA; 2019.
[52] DIANA FEA training manual. Examples for determination of boundary interfaces. Retrieved 3 June 2021. https://dianafea.com/manuals/d96/Examples/node194.html.